# Influence of Type of Loading on Fracture Behavior of High Strength Steel with Very High-Cycle Fatigue

Yusuke SANDAIJI
Materials Research Lab., Technical Development Group

*Fatigue fractures initiating in internal inclusions occurs in high-strength steel in the very high-cycle fatigue region; however, the fracture behavior under cyclic shear stress has yet to have been elucidated. This study involves ultrasonic torsional fatigue tests and ultrasonic axial fatigue tests being performed on the same bearing steel to compare the fracture behavior. The influence of the type of loading on very high-cycle fatigue characteristics is also examined. Both torsional and axial fatigue tests resulted in fractures originating in inclusions and Optically Dark Areas (ODA) were observed in the vicinity of the origins of all the fractures. However, no difference with the type of loading was recognized in the relationship between the ⊿K value, obtained from the inclusion and ODA sizes, and the number of cycles. Nevertheless, there are differences in the type of inclusions that cause fractures. It has been found that in the case of the torsional fatigue test, inclusions elongated in the rolling direction tend to be the originating points of fractures.*

## Introduction

Super high-strength steel, for example bearing steel and spring steel used in transportation machine parts and automobile engines, is known to suffer fatigue fractures that originate in non-metallic inclusions in the steel (hereinafter called "inclusions") in the very high-cycle fatigue life range of exceeding $10^7$ cycles, and many studies have been carried out to elucidate the mechanism involved.[1)-6)] It has been reported that, with very high-cycle fatigue, when a crack originating from an inclusion grows at very low speed, a characteristic area referred to as Optically Dark Area (ODA)[1)] forms around the inclusion, with its formation taking place throughout its entire lifespan.[7)] It has also been reported that the characteristics of very high-cycle fatigue are affected by both the size and type of the inclusion,[8)] however, the mechanism involved in the fracture has remained unknown.

These studies mainly took place using repeated bending stress with a rotary bending fatigue testing machine, or tensile and compressive stress with an ultrasonic axial fatigue testing machine. Meanwhile, the very high-cycle fatigue fractures in coil springs and bearings were yet to have been tested using very high-cycle fatigue life range within a practical time frame with a conventional torsional fatigue testing machine, and thus the fracture behavior and its mechanism have remained unknown. However, while the relevant studies took place due to the development of ultrasonic torsional fatigue testing machines,[9)-12)] Xue et al. performed ultrasonic axial fatigue tests and ultrasonic torsional fatigue tests on the same high-strength steel, and reported that the type of inclusion that is the origin of fractures differs in the two tests.[10)] We therefore performed ultrasonic torsional fatigue tests on bearing steel with different types of inclusions, and then reported that the crack initiation behavior depends on the type of inclusion that is the origin of the fracture.[12)]

In this paper, in order to establish material design guidelines that can be used to suppress inclusion-originating fractures in steel used which is exposed to repeated shear stress, for example coil springs and bearings, ultrasonic torsional fatigue tests under torsional load and ultrasonic axial fatigue tests under axial load were performed using bearing steel, and the fracture morphology resulting from both tests compared in examining the influence of the type of loading on inclusion-originating fatigue fracture behavior.

## 1. Experimental method

### 1.1 Test material and specimen

In making interior-originating fractures easier to occur with oxide as the originating point, an ingot based on the composition of SUJ2 bearing steel was manufactured by atmospheric melting, which increases the oxygen concentration of the molten steel, and then hot forged into a steel bar of 65 mm in diameter for use as the test material. **Table 1** shows the chemical composition of the test material. This test material was spheroiding annealing heated at 1,123 K for 20 minutes, oil quenched, and then tempered at 438 K for 150 minutes. The metallographic structure of the test material was martensite with a Vickers hardness of 698 HV at

Table 1 Chemical compositions (mass%)

| C | Si | Mn | S | Cr | Al | N | O |
|---|---|---|---|---|---|---|---|
| 0.95 | 0.25 | 0.33 | 0.0015 | 1.47 | 0.019 | 0.033 | 0.0048 |

a test load of 98 N. Mirror surface observation revealed a large number of spherical inclusions, which appeared to be oxide. The specimens used in the fatigue tests were sampled to ensure that their axial direction corresponded to the cogging direction of the test material, and then machined into the shape shown in **Fig. 1**. The torsional fatigue test used hour-glass specimens, as shown in Fig. 1 (a), and the specimens with a parallel portion, as shown in (b), were then used, in order to enable inclusion-originated fractures easier to occur by increasing the risk volume. Assuming that risk volume V corresponds to the area where 90% or more of the maximum stress was applied, then both types of the specimens used in the torsional fatigue tests would have a risk volume of 2.85 $mm^3$ and 8.71 $mm^3$, respectively, whereas the specimens used in the axial fatigue tests would have a risk volume of 33.7 $mm^3$. The specimens were mirror polished, and then shot peened to apply compressive residual stress. **Fig. 2** shows the residual stress distribution at an angle of 45° to the specimen axis measured through the X-ray diffraction method. The compressive residual stress was about 500 MPa on the specimen surface, and the maximum compressive stress about 1,200 MPa at a depth of 80 $\mu$m from the surface. The compressive stress decreased as the depth increased: being about 125 MPa at a depth of 250 $\mu$m.

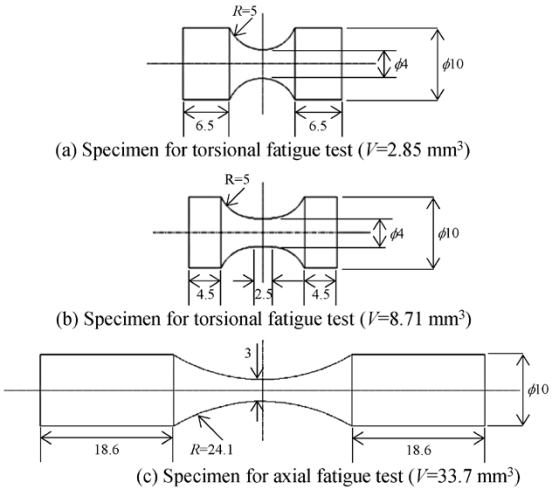


Fig. 1 Shape of specimens

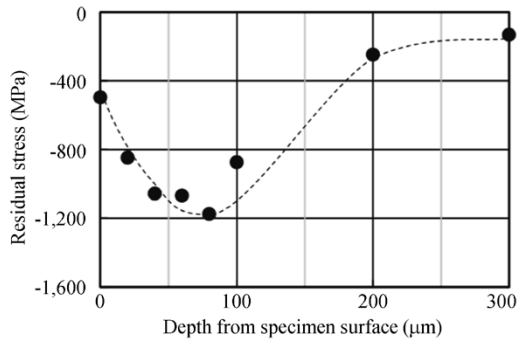


Fig. 2 Distribution of residual stress

## 1.2 Fatigue test

Both the torsional fatigue tests and axial fatigue tests were performed under alternating load and at a test frequency of 20 kHz, using ultrasonic fatigue test machines made by Shimadzu (torsional: UFT-2000T, axial: UFT-2000). Compressed air was used to suppress the heat generated during the fatigue tests. The fatigue tests also took place after having determined the intermittent test conditions, where the specimen surface temperature was maintained at below 50℃ in a preliminary test in which the oscillation stop time was varied within the range of 440 to 1,100 ms while the oscillation time was maintained at a constant of 110 ms.

## 1.3 Fracture surface observation

The fatigue fracture surface observation took place using a Scanning Electron Microscope (SEM) and an Optical Microscope (OM). The inclusion of fracture origins was identified through Energy Dispersive X-ray analysis (SEM-EDX).

The inclusion size $\sqrt{area_{inc}}$ and ODA size $\sqrt{area_{ODA}}$ were calculated using the square root of the respective areas measured through image analysis, namely SEM images and OM images from a direction perpendicular to the fracture surface.

# 2. Experimentation results

## 2.1 Fatigue test results

**Fig. 3** shows the S-N curve. The open plots in the figure represent the surface-originating fractures while the solid plots represent the interior-originating fractures. The alphabetical notations represent the type of inclusion of the origin of the

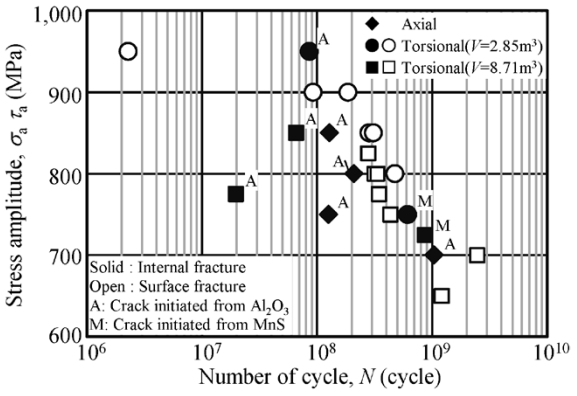


Fig. 3 Results of fatigue tests

fracture: A standing for $Al_2O_3$ based inclusions and M for MnS based inclusions, etc. The S-N curve under torsional load indicated an increase in the number of cycles with decreased stress amplitude, and no influence of the risk volume was observed apart from the fracture point at approximately $2x10^7$ cycles that had a stress amplitude $\tau_a$ of 775 MPa. According to the fracture surface observation results, which will be described at a later stage, there were a mixture of interior-originating factures and surface-originating fractures. Sakanaka et al. performed ultrasonic torsion fatigue tests using bearing steel without shot peening, and reported that only surface-originating fractures occur at a cycle number of $10^5$ to $10^9$.[13] With respect to this paper, interior-originating fractures seem to have occurred more easily because of the increased number of inclusions due to atmospheric melting and hardened surfaces resulting from the shot peening. Meanwhile, under axial load, the number of cycles increased with decreased stress amplitude, and with all the fractures being of the interior-originating type.

In focusing on the inclusion-originating fracture behavior, this paper will describe the test results where inclusion-originating fractures actually occurred. No influence from the risk volume was observed with torsional fatigue tests specimens and therefore the test results of both types of specimens are handled without distinction.

### 2.2 Fracture surface observation results

**Fig. 4** shows an overview of the fractured specimens from the torsional fatigue tests, where the inclusion-originating fractures occurred. Under torsional load the cracks grew at an angle of 45° to the specimen axis, i.e. in a perpendicular direction to the direction of the maximum principal stress, and therefore the fracture seems to have been caused by the principal stress type crack growth. **Fig. 5** shows SEM and OM images around the origin. All the interior-originating fractures initiated in inclusions, and ODAs were observed around every fracture origin inclusion, excluding the specimen that fractured at $2x10^7$ cycles under torsional load. When a crack grows in the maximum shear stress direction under torsional load, the fracture surfaces get smoothed out due to the abrasion between them. In this study, however, no smooth fracture surfaces were observed around the origin, but an ODA was observed in the same way as under axial load; therefore, giving rise to the conclusion that fatigue cracks grew due to the maximum principal stress.

Meanwhile, under axial load, an ODA was observed around the inclusion, and the fracture occurred due to principal stress type crack growth in the same way as reported in the past.[1), 4), 6), 7)]

**Fig. 6** shows the relationship between the inclusion size $\sqrt{area}_{inc}$ and the number of cycles $N$. Fractures occurred with inclusions of $\sqrt{area}_{inc}$ = 10 to 80 $\mu$m as the originating points under torsional load and fractures occurred with inclusions of $\sqrt{area}_{inc}$ = 5 to 20 $\mu$m as the originating points under axial load, and hence the $\sqrt{area}_{inc}$ value did not significantly depend on the fatigue life once over $10^8$ cycles. **Fig. 7** shows the relationship between the ODA size $\sqrt{area}_{ODA}$ and number of cycles N. ODAs of $\sqrt{area}_{ODA}$ = 30 to 60 $\mu$m formed under torsional load

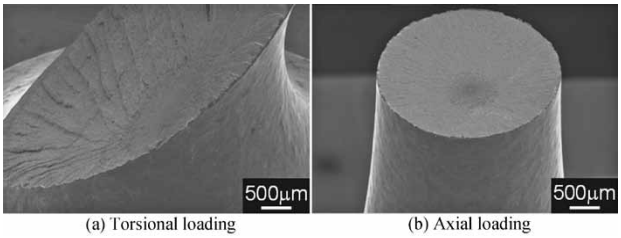


Fig. 4 Overview of fractured specimens

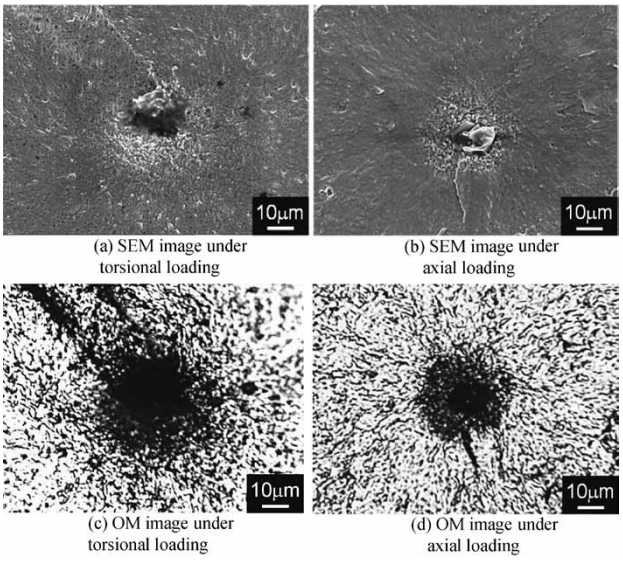


Fig. 5 Overview of fractured specimens

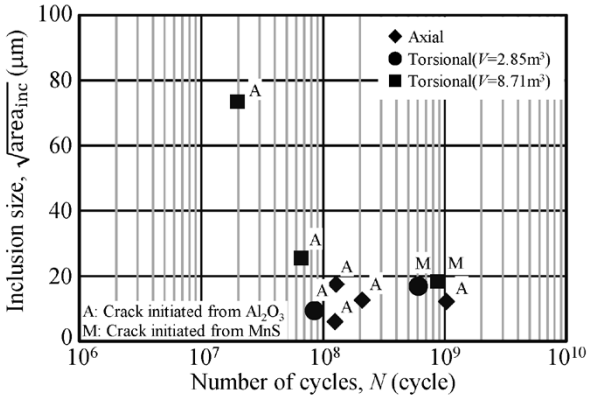


Fig. 6 Relationship between number of cycles and inclusion size

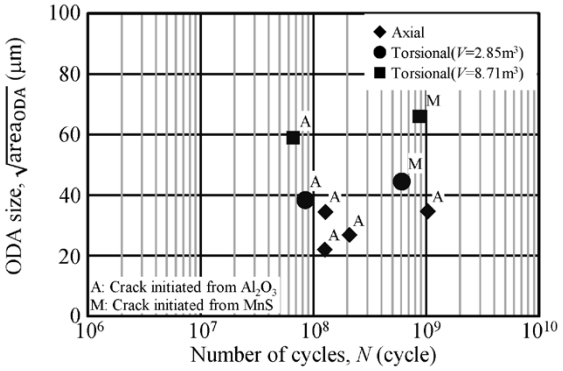


Fig. 7 Relationship between number of cycles and ODA size

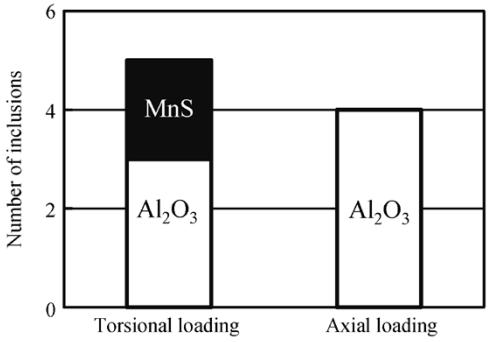


Fig. 8 Type of fracture origin inclusions

and ODAs of $\sqrt{area_{ODA}}$ = 20 to 40 $\mu$m formed under axial load, and hence no significant correlation was observed between the number of cycles and $\sqrt{area_{ODA}}$ value.

**Fig. 8** shows the type of fracture origin inclusion. Under axial load, all the fractures occurred with $Al_2O_3$ based inclusions as the originating point, whereas under torsional load, the fractures occurred with $Al_2O_3$ based inclusions and MnS based inclusions as the originating points, being basically half and half.

## 3. Discussion

### 3.1 Influence of loading type on crack initiation behavior

In addition to $Al_2O_3$ based inclusions, MnS based inclusions were also the fracture origins under torsional load. Based on cross-sectional observation of the fracture origins, we have previously reported that, under torsional load, principal stress type cracks initiate, grow, and then lead to fractures in the case of $Al_2O_3$ based inclusions, whereas shear type cracks initiate, change to principal stress type cracks, and then lead to fractures in the case of MnS based inclusions.[12] In the latter case, the shear type cracks originate from inside MnS based inclusions elongated in the direction of the maximum shear stress, and hence it would appear that the shear type cracks occurred as a result of their projection area in the direction of the maximum shear stress increasing. In this study, the specimens were sampled so that their axial direction would correspond to the cogging direction of the steel material; therefore, the MnS inclusions are elongated in the direction of the maximum shear stress. It would therefore appears that some of them became the originating points of the fractures. Meanwhile, under axial load, it would appear that they did not become the fracture origin because their projection area in the maximum principal stress direction decreased.

### 3.2 Influence of loading type on crack growth

In order to examine the influence of the loading type on the crack growth, the number of cycles was compared with the stress intensity factor range $\Delta K$, which were obtained from the size of the inclusion of the fracture origin and the ODA, under torsional load and axial load, respectively. **Fig. 9** and **Fig.10** show the relationship between the number of cycles and $\Delta K_{inc}$ and $\Delta K_{ODA}$ values, which were obtained from the size of the the fracture origin inclusion and the ODA, respectively. $\Delta K_{inc}$ and $\Delta K_{ODA}$ were calculated using Equation (1) by substituting $\sqrt{area_{inc}}$ and $\sqrt{area_{ODA}}$ for $\sqrt{area}$, respectively.

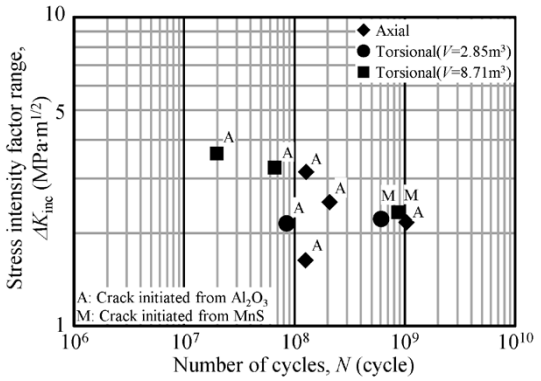


Fig. 9 Relationship between number of cycles and $\Delta K_{inc}$

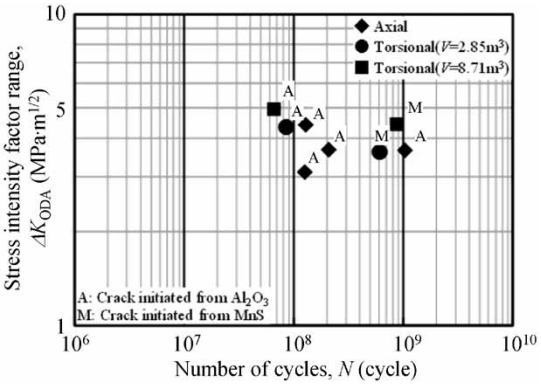


Fig.10 Relationship between number of cycles and $\Delta K_{ODA}$

$$\Delta K = 0.5 \Delta \sigma \sqrt{\pi \sqrt{area}} \quad \cdots\cdots (1)$$

Where, $\Delta\sigma$ represents the stress range applied to a crack, which was obtained by substituting the stress amplitude, assuming that only the tensile component affects the crack growth. The torsional fatigue test took place under alternating load, where the resulting fractures indicate that the cracks grew in the direction perpendicular to the maximum principal stress $\sigma_{pr.}$ as described above. For this reason, using the assumption that Equation (2) can be established, the principal stress amplitude $\sigma_{pr.eff.a}$ was obtained using Equation (3) in consideration of the stress gradient, and then $\Delta K$ by substituting the resulting value into Equation (1).

$$\sigma_{pr.a} = \tau_a \quad \cdots\cdots (2)$$

$$\sigma_{pr.eff.a} = \tau_a (1 - D/R) \quad \cdots\cdots (3)$$

Where, $\tau_a$ represents the maximum shear stress amplitude on the specimen surface, $D$ the depth of the origin from the specimen surface, and $R$ the radius of the specimen.

Under torsional load, $\Delta K_{inc}$ decreases with an increase in number of cycles (Fig. 9); however, $\Delta K_{ODA}$ does not depend on the number of cycles, and remains substantially constant in the range of 3 to 5 MPa-m$^{1/2}$, and thus indicating there to be no difference in the inclusion type (Fig.10). This tendency and the $\Delta K_{ODA}$ value correspond to those under axial load, in the same way as described in a previous report.[2] This indicates that the cracks grow very slowly while forming ODAs in the same way under axial load and bending load, but then changes to general crack growth without forming any ODAs when $\Delta K_{ODA}$ reaches a certain value, and this is because the principal stress type crack growth occurs under alternating torsional load. This means that principal stress type cracks or shear type cracks may depend on the shape of the inclusion when inclusion-originating fractures occur under torsional load; however, the fractures are caused by the principal stress type crack growth in both cases. Once an ODA has formed around the origin and $\Delta K_{ODA}$ reaches a certain value, it then changes to general crack growth, and ultimately a fracture. It has been reported that most of the entire number of cycles is spent on the crack growth that forms ODAs under axial load.[7] It would appear that this crack growth dominates the fatigue life in the same way even under torsional load. For this reason, we will aim at establishing structure design guidelines by clarifying the metallographic factors that suppress such crack growth. In addition, a study is necessary from the viewpoint of not only the metallographic structure but also inclusion control as it would appear that the shape and hardness of the inclusion affects the crack initiation life, because the crack initiation behavior depends on the shape of the inclusion under torsional load.

## Conclusions

Ultrasonic torsional fatigue tests and ultrasonic axial fatigue tests using bearing steel were performed, and the fracture behavior under torsional load and axial load compared, thereby examining the influence of the type of loading on inclusion-originating fracture behavior. The result included the following discoveries.

(1) With crack initiation under torsional load, fatigue fractures occurred with elongated inclusions, such as MnS based inclusions, as the originating point.

(2) With crack growth under torsional load, principal stress type cracks grow with the formation of ODA around the inclusions, regardless of the type of inclusion that causes the fracture, and when $\Delta K_{ODA}$ reaches a certain value, it changes to general crack growth, and then leads to fractures.

(3) The $\Delta K_{ODA}$ values under torsional load and axial load are comparable. Presumably, this is because the principal stress type crack growth occurred under both types of loading.

## References


1) Y. Murakami et al. *Fatigue & Fracture of Engineering Materials & Structures*. 1999, Vol.22, p.581.
2) K. Tanaka et al. *Fatigue & Fracture of Engineering Materials & Structures*. 2002, Vol.25, p.775.
3) C. Bathias. *Fatigue & Fracture of Engineering Materials & Structures*. 1999, Vol.22, p.559.
4) H. Mayer et al. *International Journal of Fatigue*. 2009, Vol.31, p.242.
5) K. Shiozawa et al. *Fatigue & Fracture of Engineering Materials & Structures*. 2001, Vol.24 , p.781.
6) T. Sakai et al. *Fatigue & Fracture of Engineering Materials & Structures*. 2001, Vol.25, p.765.
7) W. Ishida et al. *Transactions of the Japan Society of Mechanical Engineers A*. 2012, Vol.78, p.23.
8) Y. Furuya et al. *Metallurgical and Materials Transactions A*. 2007, Vol.38, p.1722.
9) S. E. Stanzl-Tschegg et al. *Ultrasonics*. 1993, Vol.31, p.275.
10) H. Q. Xue et al. *Engineering Fracture Mechanics*. 2010, Vol.77, p.1866.
11) Y. Shimamura et al. *International Journal of Fatigue*. 2014, Vol.60, p.57.
12) Y. Sandaiji et al. *Procedia Materials Science*. 2014, Vol.3, p.894.
13) N. Sakanaka et al. *NTN TECHNICAL REVIEW*. 2011, Vol.79, p.104.